

Supplementary Materials for

A helical inner scaffold provides a structural basis for centriole cohesion

Maeva Le Guennec, Nikolai Klena, Davide Gambarotto, Marine H. Laporte, Anne-Marie Tassin, Hugo van den Hoek, Philipp S. Erdmann, Miroslava Schaffer, Lubomir Kovacik, Susanne Borgers, Kenneth N. Goldie, Henning Stahlberg, Michel Bornens, Juliette Azimzadeh, Benjamin D. Engel*, Virginie Hamel*, Paul Guichard*

*Corresponding author. Email: ben.engel@helmholtz-muenchen.de (B.D.E.); virginie.hamel@unige.ch (V.H.); paul.guichard@unige.ch (P.G.)

Published 14 February 2020, *Sci. Adv.* **6**, eaaz4137 (2020)
DOI: 10.1126/sciadv.aaz4137

The PDF file includes:

- Fig. S1. Visualization of the connections between MTTs in cryo-tomograms.
- Fig. S2. MTT to MTD transitions.
- Fig. S3. The inner scaffold maintains centriole cohesion under compressive forces.
- Fig. S4. Reconstruction resolutions and computational pipeline for reconstructing the complete central region.
- Fig. S5. Assessing the correctness of the structure: Raw images versus averages.
- Fig. S6. Periodicity of the inner scaffold stem in *P. tetraurelia*, *C. reinhardtii*, *N. gruberi*, and humans.
- Fig. S7. Periodicity, helicity, and de novo subtomogram averaging.
- Fig. S8. Optimized U-ExM protocol in human cells reveals components of the inner scaffold.
- Fig. S9. POC1B, FAM161A, POC5, and Centrin-2 colocalize with the inner scaffold structure as simulated U-ExM fluorescence.
- Fig. S10. 3D localization of the inner core proteins and extended localization of GFP-POC1B at the proximal region of the centriole upon overexpression.
- Legends for movies S1 to S6
- Legends for data files S1 and S2
- Reference (40)

Other Supplementary Material for this manuscript includes the following:

(available at advances.sciencemag.org/cgi/content/full/6/7/eaaz4137/DC1)

- Movie S1 (.avi format). Cryo-tomogram of a *P. tetraurelia* centriole ex vivo.
- Movie S2 (.avi format). Cryo-tomogram of a *C. reinhardtii* centriole in situ.
- Movie S3 (.mov format). 3D representation of the *P. tetraurelia* central core highlighting the helical pattern of the inner scaffold.

Movie S4 (.mov format). 3D representation of the *C. reinhardtii* central core highlighting the helical pattern of the inner scaffold.

Movie S5 (.mov format). 3D rendering of the full central core architecture from *P. tetraurelia*.

Movie S6 (.mov format). 3D rendering of the full central core architecture from *C. reinhardtii*.

Data file S1 (.tif format). The complete central core reconstruction from *P. tetraurelia*.

Data file S2 (.tif format). The complete central core reconstruction from *C. reinhardtii*.

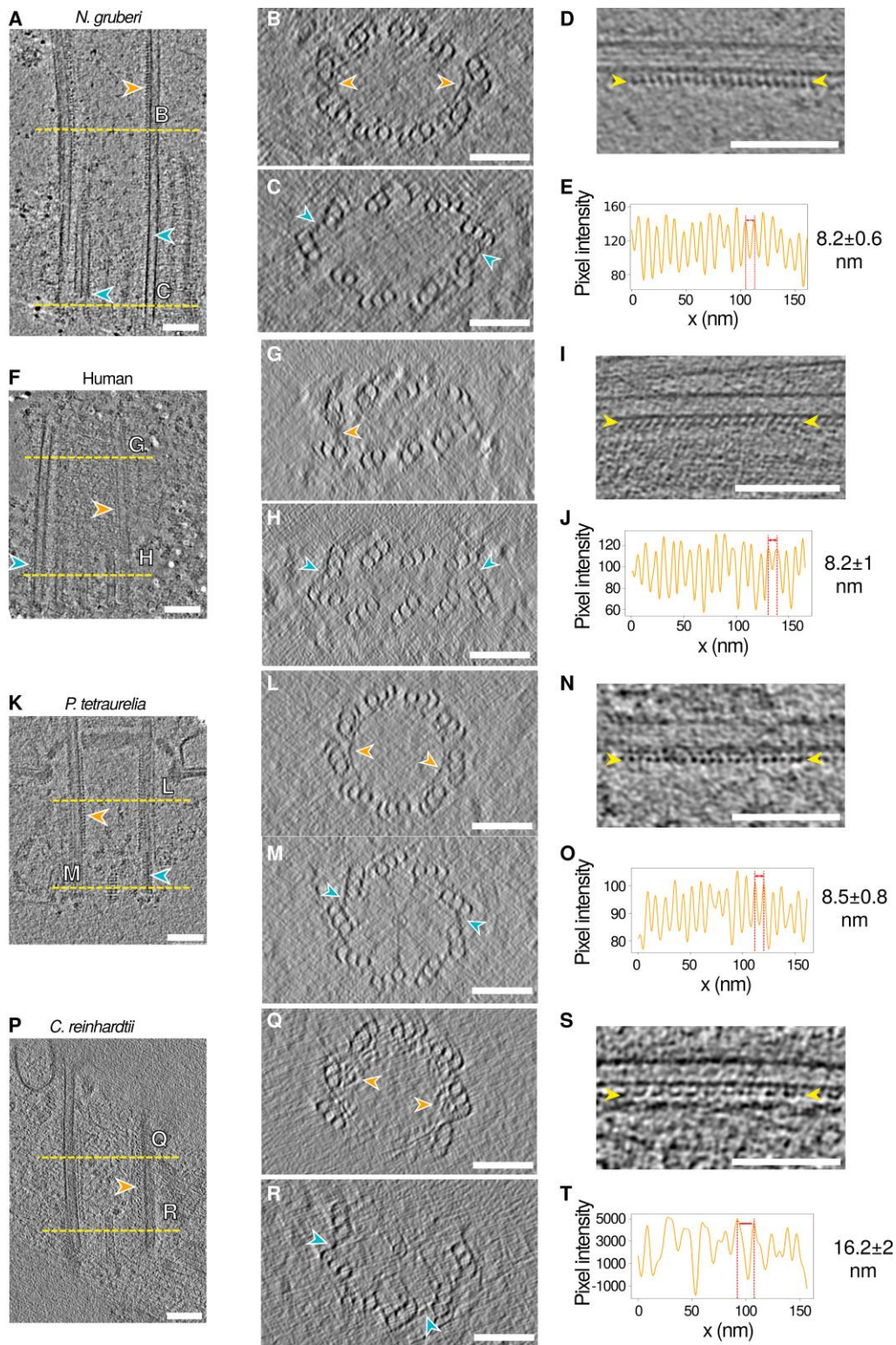


Fig. S1. Visualization of the connections between MTTs in cryo-tomograms. (A, F, K, P) Cryo-ET of longitudinal central sections through (A) *Naegleria gruberi*, (F) human, (K) *Paramecium tetraurelia* and (P) *Chlamydomonas reinhardtii* centrioles.

Yellow dashed lines indicate the respective positions of cross-sections (**B**, **C**: *N. gruberi*; **G**, **H**: human; **L**, **M**: *P. tetraurelia*; **Q**, **R**: *C. reinhardtii*). Orange arrowheads: inner scaffold; Turquoise arrowheads: A-C linker. Note that due to the tomographic missing wedge, we do not see the entire circular structure of the inner scaffold. (**D**, **I**, **N**, **S**) Longitudinal zoomed-in views of inner scaffold densities attached to MTTs (**D**: *N. gruberi*; **I**: human; **N**: *P. tetraurelia*; **S**: *C. reinhardtii*) and their corresponding line intensity profiles (**E**, **J**, **O** and **T**, respectively) showing average periodicities. Yellow arrowheads: ends of the lines used to plot intensity profiles. Scale bars: 100 nm.

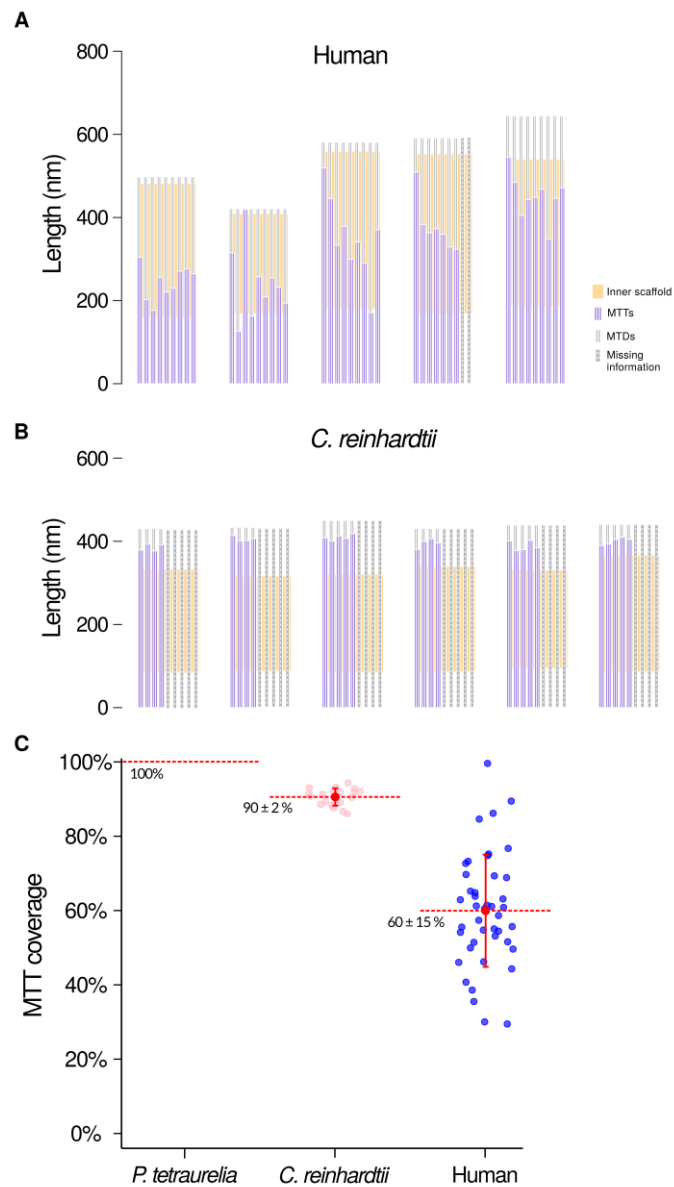


Fig. S2. MTT to MTD transitions. (A) Schematic distribution of MTTs and MTDs along the length of human centrioles. (B) Schematic distribution of MTTs and MTDs along the length of *C. reinhardtii* centrioles. The end of the centriole is defined by the appearance of the stellate structure. The centrioles are incomplete (missing information) because they are not entirely contained within the 100-200 nm-thick FIB-milled lamellas. (C) Average MTT coverage in *P. tetraurelia*, *C. reinhardtii* and human centrioles. Note that microtubule doublets were never observed in *P. tetraurelia* centrioles, resulting in an MTT coverage of 100%.

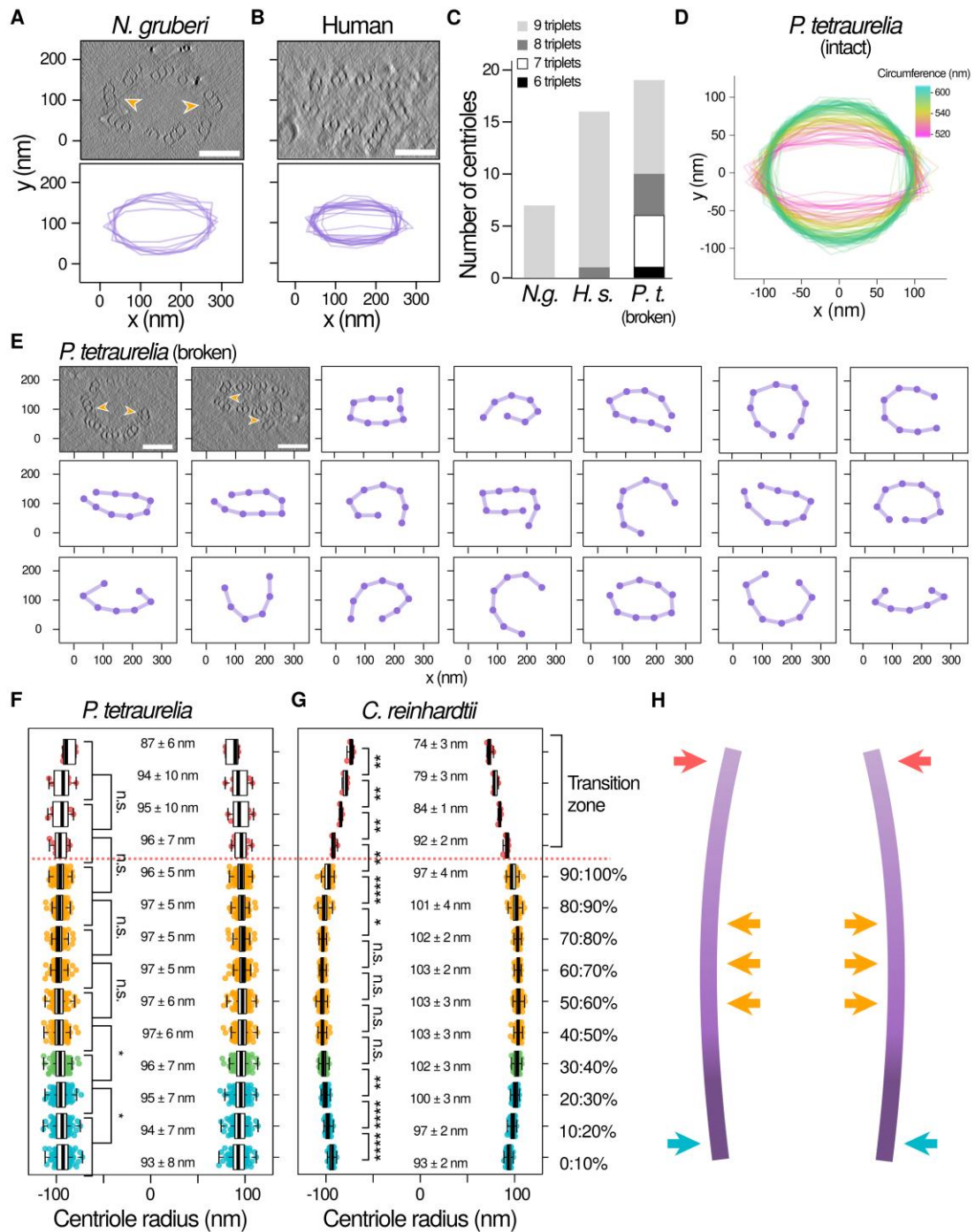


Fig. S3. The inner scaffold maintains centriole cohesion under compressive forces. (A, B) Representative top views of compressed centrioles from (A) *N. gruberi* and (B) human cells. Orange arrowheads: inner scaffold. Note that due to the tomographic missing wedge, we do not see the entire circular structure of the inner scaffold. Bottom panels show the circumferential shapes of 7 *N. gruberi* and 17 human centrioles, represented as polygons with each vertex corresponding to the

coordinates of an A-microtubule. **(C)** Quantification of the number of MTTs in *N. gruberi* centrioles (*N.g.*), human centrioles (*H.s.*) and broken *P. tetraurelia* centrioles (*P.t.*). **(D)** Circumferential shapes of central regions from 65 intact *P. tetraurelia* centrioles. Centriole plots are colored according to their circumference (calculated as the sum of distances between adjacent A-microtubules). **(E)** Geometry and MTT connectivity of broken *P. tetraurelia* centrioles. The purple line indicates an inner scaffold connection between MTTs, and a discontinuous line indicates the loss of connection between MTTs. **(F, G)** Centriole radius in **(F)** *P. tetraurelia* and **(G)** *C. reinhardtii* along the centriolar length. The radius was measured as the distance between the centriole center and the center of the A-microtubule in 10 *P. tetraurelia* and 6 *C. reinhardtii* centrioles, with transition zones measured on 2 and 1 centriole, respectively. **(H)** Schematic representation of the change in centriole radius caused by hypothetical forces within the *C. reinhardtii* cell (red and blue arrows) that are resisted by the inner scaffold (orange arrows), resulting in a barrel-shaped centriole. Scale bars: 100 nm.

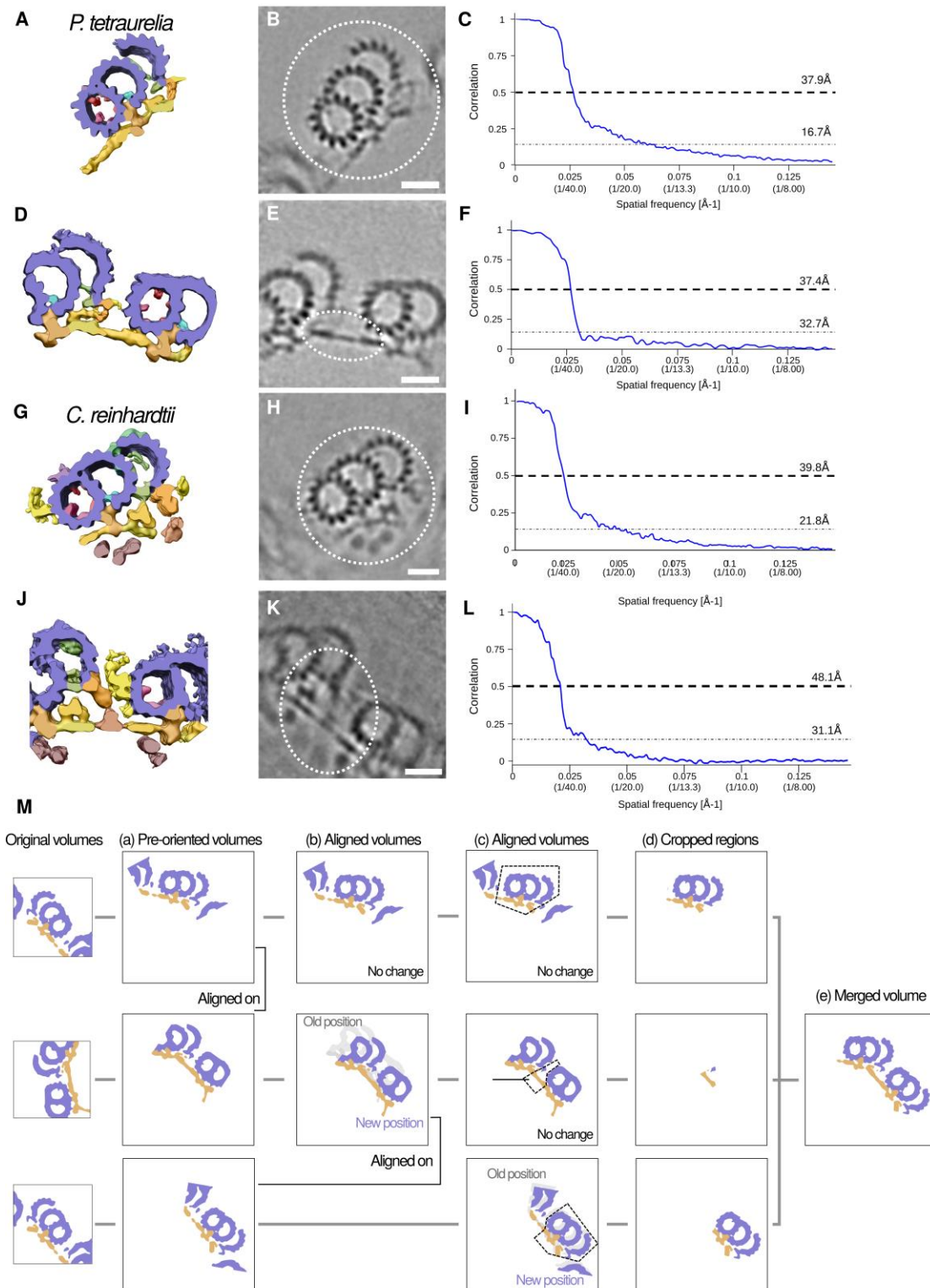


Fig. S4. Reconstruction resolutions and computational pipeline for reconstructing the complete central region. (A, D, G, J) Reconstructed 3D maps of the (A) MTTs from the *P. tetraurelia* central region, (D) junction from the *P. tetraurelia* central region, (G) MTTs from the *C. reinhardtii* central region and (J)

junction from the *C. reinhardtii* central region. (**B, E, H, K**) Corresponding 2D views of the reconstructed maps. A mask (white dashed line) was applied to focus on the region of interest to compute the resolution estimation. (**C, F, I, L**) Resolution estimation using Fourier Shell Correlation (FSC) curves. (**M**) Computational pipeline used to generate the combined maps (see Materials and Methods). Scale bars: 20nm.

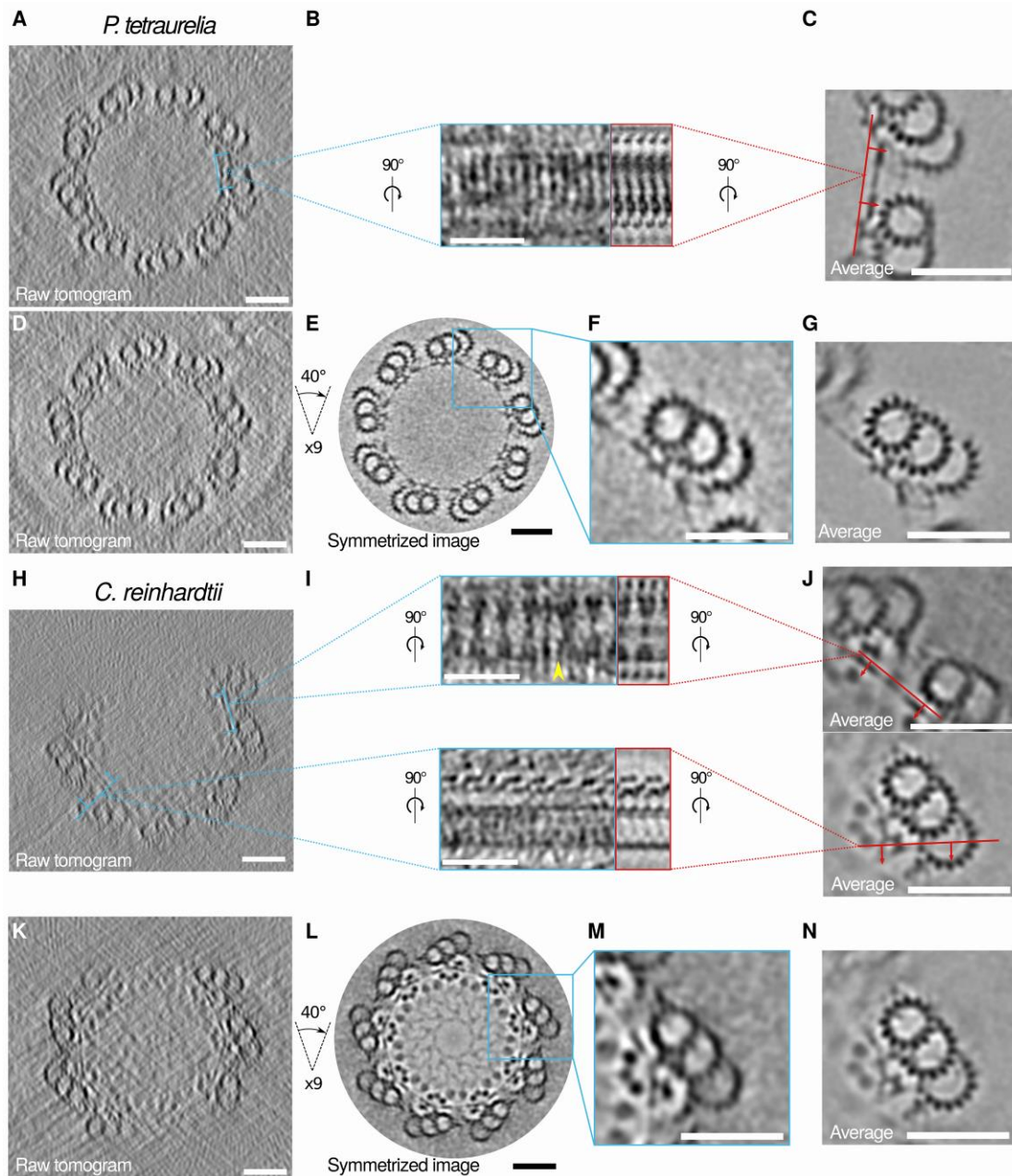


Fig. S5. Assessing the correctness of the structure: Raw images versus averages.

(A, D) Cross-section top views of *P. tetraurelia* centrioles from raw tomograms. (B) Longitudinal reslice of the raw tomogram along the junction as indicated by the blue line in panel A (left), and corresponding reslice of the reconstructed junction following the red line from panel C (right). (C) Reconstructed map of the *P. tetraurelia* junction. (E) Circularization and symmetrization of the image in panel D using centrioleJ plugin from ImageJ. (F) Zoom-in on a triplet from panel E. (G) Reconstructed map of *P. tetraurelia* triplet. (H, K) Cross-section top views of

Chlamydomonas reinhardtii centrioles from raw tomograms. **(I)** Longitudinal reslices along the junction (top, left) and along the C-MT (bottom, left) as indicated by the blue lines in panel **H**, and corresponding reslices of the reconstruction along the junction (top, right) and along the C-MT (bottom, right) as indicated by the red lines from panel **J**. Yellow arrowhead points to a gap. **(J)** Reconstructed maps of the *C. reinhardtii* junction (top) and MTT (bottom). **(L)** Circularization and symmetrization of the image in panel **K** using centrioleJ plugin from ImageJ. **(M)** Zoom-in on a MTT from panel **L**. **(N)** Reconstructed map of *C. reinhardtii* triplet. Scale bars: 50 nm.

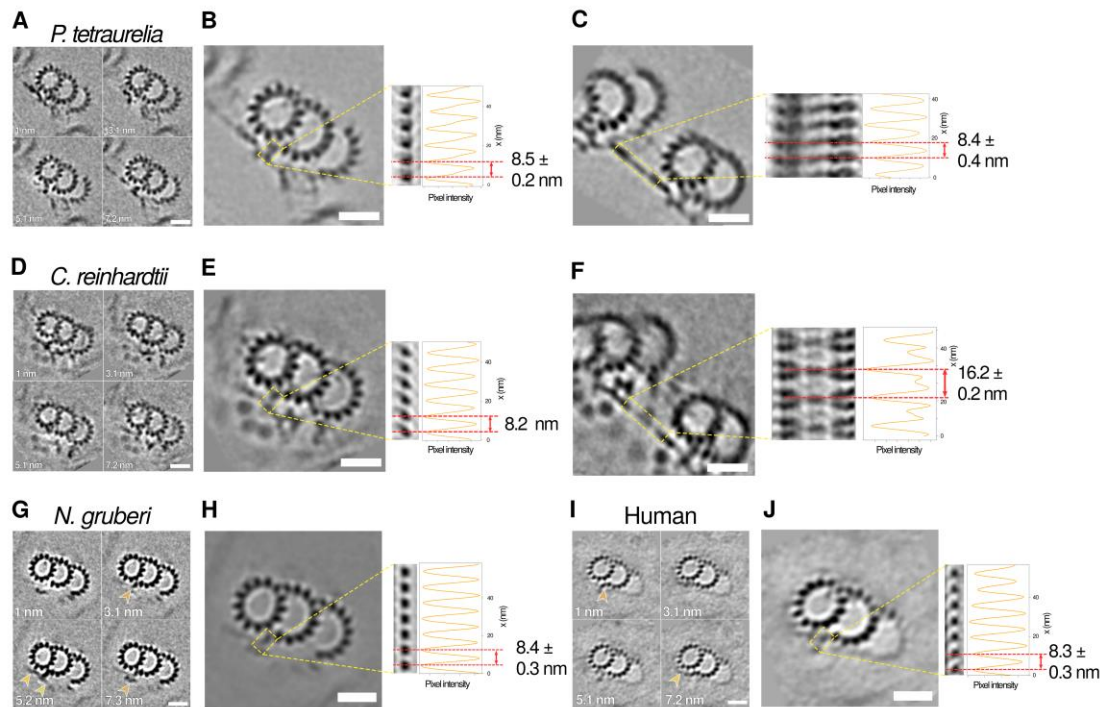


Fig. S6. Periodicity of the inner scaffold stem in *P. tetraurelia*, *C. reinhardtii*, *N. gruberi*, and humans. (A, D, G, I) Sequential Z-projections through reconstructed maps of MTTs from (A) *P. tetraurelia*, (D) *C. reinhardtii*, (G) *N. gruberi* and (I) human. Each image has a thickness of 2 nm. (B, E, H, J) Z-projections (thickness of 60 nm) of the same reconstructed MTTs (left panel) and side view of the stem (middle panel) with its corresponding line intensity profile (right panel) for (B) *P. tetraurelia*, (E) *C. reinhardtii*, (H) *N. gruberi* and (J) human. (C, F) Z-projection (thickness of 60 nm) of the reconstructed junctions (left panel) and side view of the junction (middle panel) with its corresponding line intensity profile (right panel) for (C) *P. tetraurelia* and (F) *C. reinhardtii*. Scale bars: 20nm.

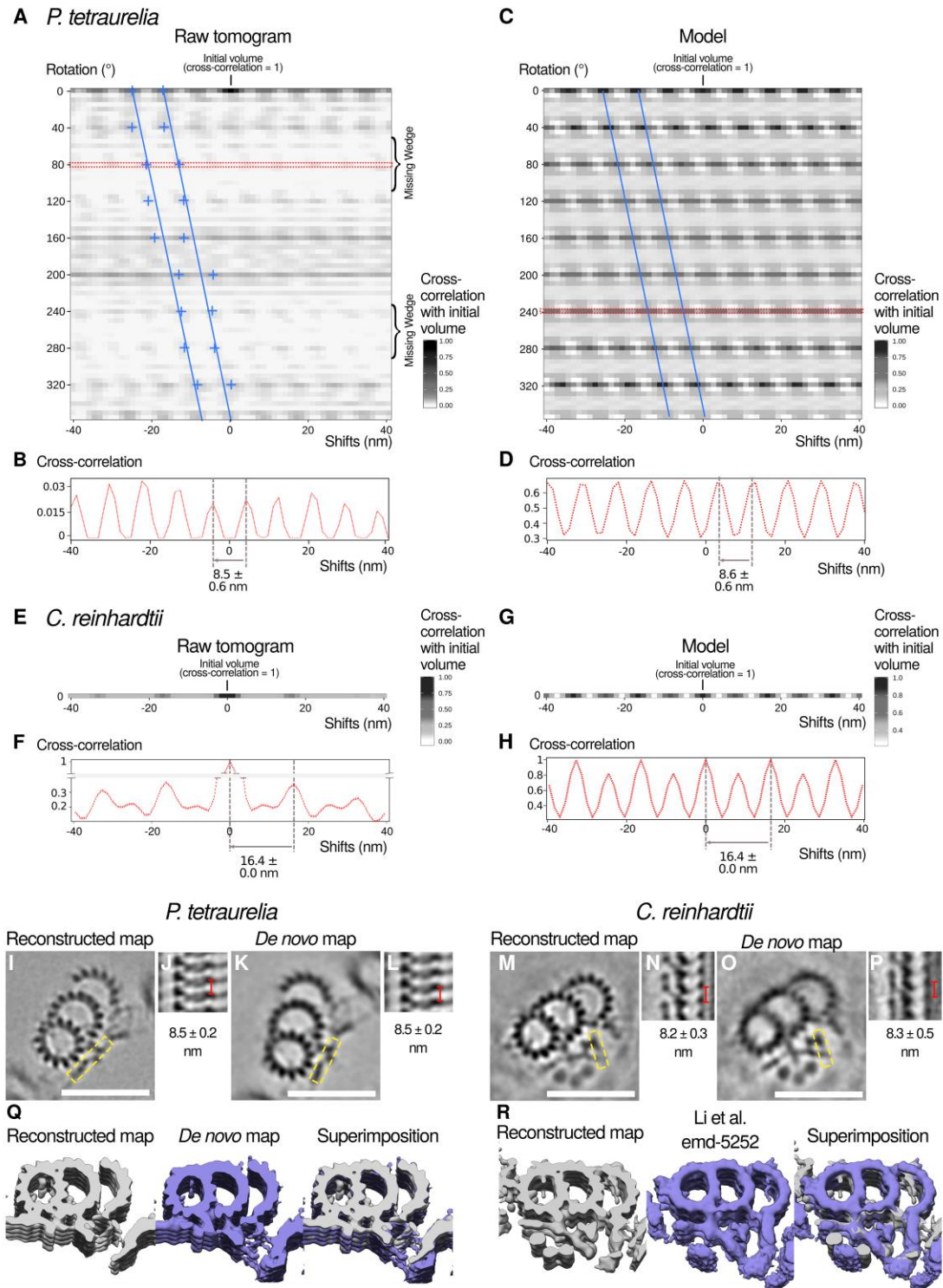


Fig. S7. Periodicity, helicity, and de novo subtomogram averaging. (A-H)

Translational and rotational analysis of the inner scaffold in *P. tetraurelia* and *C. reinhardtii* centrioles. (A) Autocorrelation heatmap from a cross-section of the inner scaffold from a *P. tetraurelia* raw tomogram correlated with itself after rotations

and/or shifts were applied to the volume either around or along the z-axis, respectively. The tomographic missing wedge lacks structural features, resulting in some white areas where the cross-correlation values are lower between the initial volume and its rotated version. Blue crosses indicate the positions of cross-correlation peaks. Blue lines are manually fitted lines to the blue crosses, showing the pattern of a 2-start helix in the structure. (B) Plot profile of the autocorrelation between the original volume and its version rotated by 80 degrees and shifted along the z-axis. (C) Autocorrelation heatmap from a cross-section of the inner scaffold from the *P. tetraurelia* model correlated with itself after rotations and/or shifts were applied. Blue lines are manually fitted to the cross-correlation peaks, showing the pattern of a 2-start helix in the structure. (D) Plot profile of the autocorrelation between the original volume and its version rotated by 240 degrees and shifted along z. (E) Autocorrelation heatmap of a cross-section of the inner scaffold from a *C. reinhardtii* raw tomogram correlated with itself after shifts were applied. Shifts were applied to the volume along the z-axis. As centrioles obtained in FIB-milling are not complete, the rotational analysis could not be performed reliably. (F) Plot profile of the autocorrelation between the original volume and its version shifted along z. (G) Autocorrelation heatmap of a cross-section of the inner scaffold from the *C. reinhardtii* model correlated with itself after shifts were applied. Shifts were applied to the volume along z-axis. (H) Plot profile of the autocorrelation between the original volume and its version shifted along z. **(I, K, M, O)** Z-projection of 100 slices from *P. tetraurelia* or *C. reinhardtii* subtomogram averages reconstructed either (I, M) using a reference or (K, O) *de novo* (reference free). **(J, L, N, P)** Side views corresponding to the yellow boxed in regions from I, K, M, O highlighting the periodicity of the inner scaffold, which is preserved regardless of starting reference.

Scale bars: 50nm. **(Q)** Three-dimensional views of *P. tetrauralia* maps reconstructed with reference (left) or *de novo* (middle) and superimposition of both maps (right).

(R) Three-dimensional views of *C. reinhardtii* maps reconstructed with reference (left) or *de novo* from Li. et al (**U**, EMD code: 5252; middle) and superimposition of both maps (right).

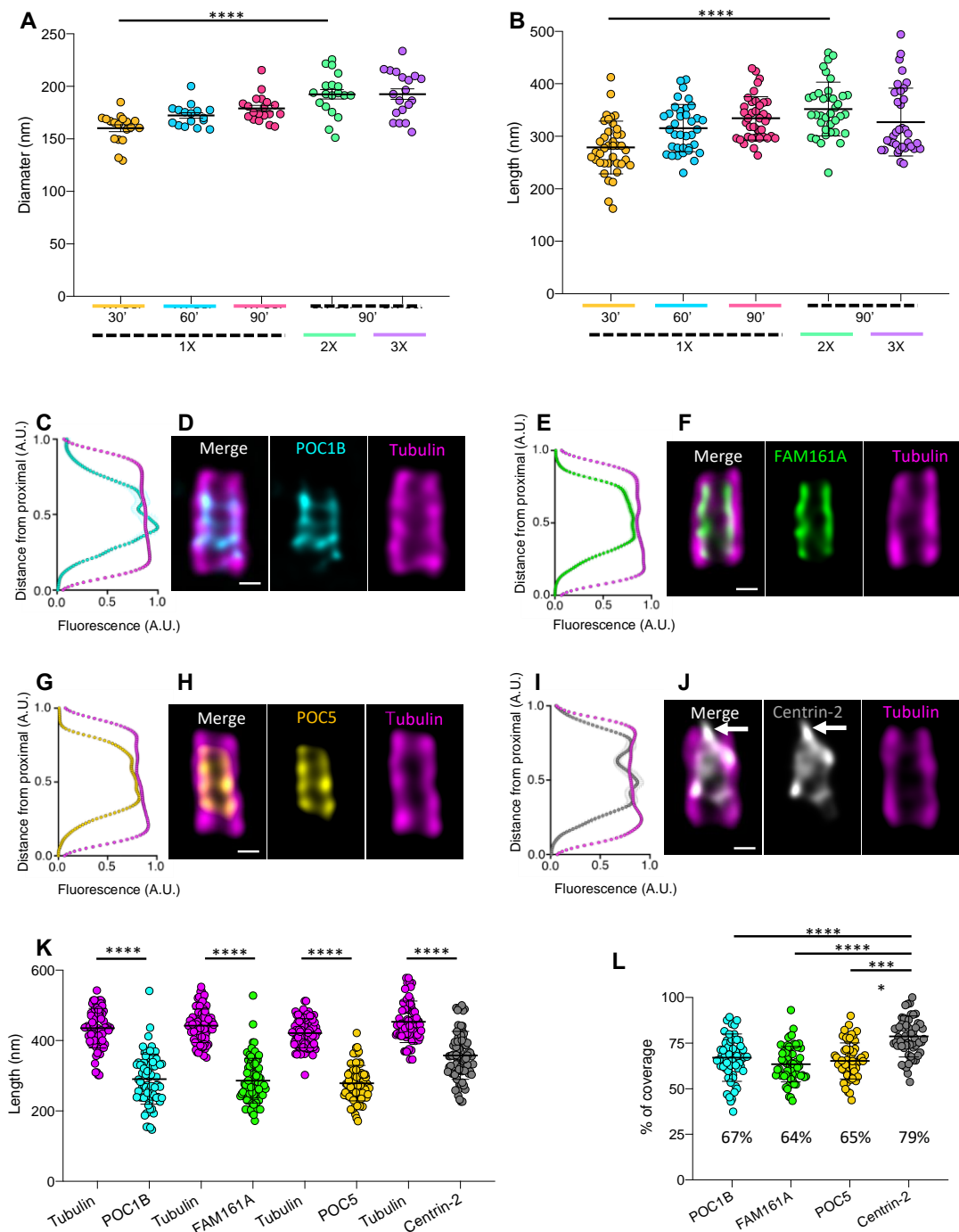


Fig. S8. Optimized U-ExM protocol in human cells reveals components of the inner scaffold. Quantification of polyglutaminated-tubulin (A) length and (B) diameter of in situ expanded human centrioles incubated in the different conditions of AA/FA concentration and denaturation time, as indicated on the X-axis (1X 30 min, 1X 60 min, 1X 90 min, 2X 90 min or 3X 90 min). Average and standard deviation for

diameters are in nm as follows: 160.2 (+/-13.8), 172.3 (+/-10.5), 179.0 (+/-12.7), 192.5 (+/-19.9), 192.5 (+/-21.6) for **1X 30'**, **1X 60'**, **1X 90'**, **2X 90'** and **3X 90'**, respectively. N= 18, 16, 19, 19, 19 centrioles for **1X 30'**, **1X 60'**, **1X 90'**, **2X 90'** and **3X 90'**, respectively. Average and standard deviation for length are in nm as follows: 278.7 (+/-50.2), 315.7 (+/-45.1), 334.2 (+/-41.3), 355.4 (+/-47.5), 327.0 (+/-64.6) for **1X 30'**, **1X 60'**, **1X 90'**, **2X 90'** and **3X 90'**, respectively. N= 39, 36, 38, 36, 35 centrioles for **1X 30'**, **1X 60'**, **1X 90'**, **2X 90'** and **3X 90'**, respectively. Data are collected from two independent experiments. Statistical significance was assessed by one-way ANOVA followed by Tukey's posthoc test ****= $p < 0.0001$. (**C, E, G, I**)

Fluorescence intensity profiles of tubulin (magenta) and the inner core proteins along the centriole length from proximal (y-axis= 0) to distal (y-axis= 1). Fluorescence intensity is expressed as the ratio relative to the maximal peak measured both for tubulin and the inner scaffold protein (cyan: POC1B; green: FAM161A; yellow: POC5 and grey: Centrin-2). n= 57, 59, 57 and 60 centrioles for POC1B, FAM161A, POC5 and Centrin-2 respectively, from 3 independent experiments (**D, F, H, J**)

Representative Lightning confocal images of *in situ* expanded mature human centrioles (longitudinal views) co-stained for tubulin (magenta) and the indicated inner scaffold proteins (color code is as above). White arrow in (**J**) indicates the additional distal localization of Centrin-2. Scale bar: 100 nm. (**K**) Quantification of tubulin (magenta) and inner scaffold protein (color code as above) fluorescent signal length in nm. Averages (+/- standard error of the mean) are as follows: 435 (+/-7.4) and 291 (+/-9.7) for tubulin and POC1B, 442 (+/-6.4) and 286 (+/-7.3) for tubulin and FAM161A, 421 (+/-5.4) and 279 (+/-7.0) for tubulin and POC5, 454 (+/-7.5) and 358 (+/-8.6) for tubulin and Centrin-2. N= 57, 59, 57 and 60 centrioles for POC1B, FAM161A, POC5 and Centrin-2, respectively, from 3 independent experiments.

Statistical significance was assessed by one-way ANOVA followed by Tukey's posthoc test, ****= $p < 0.0001$ for each condition. (L) Percentage coverage of the inner scaffold proteins relative to tubulin. Average (+/- standard error of the mean) are as follow: 67% (+/-1.7), 64% (+/-1.3), 65% (+/-1.3) and 79% (+/-1.4) for POC1B, FAM161A, POC5 and Centrin-2, respectively. N= 57, 59, 57 and 60 centrioles for POC1B, FAM161A, POC5 and Centrin-2, respectively, from 3 independent experiments. Statistical significance was assessed by one-way ANOVA followed by Tukey's posthoc test, **** = $p < 0.0001$ for each condition.

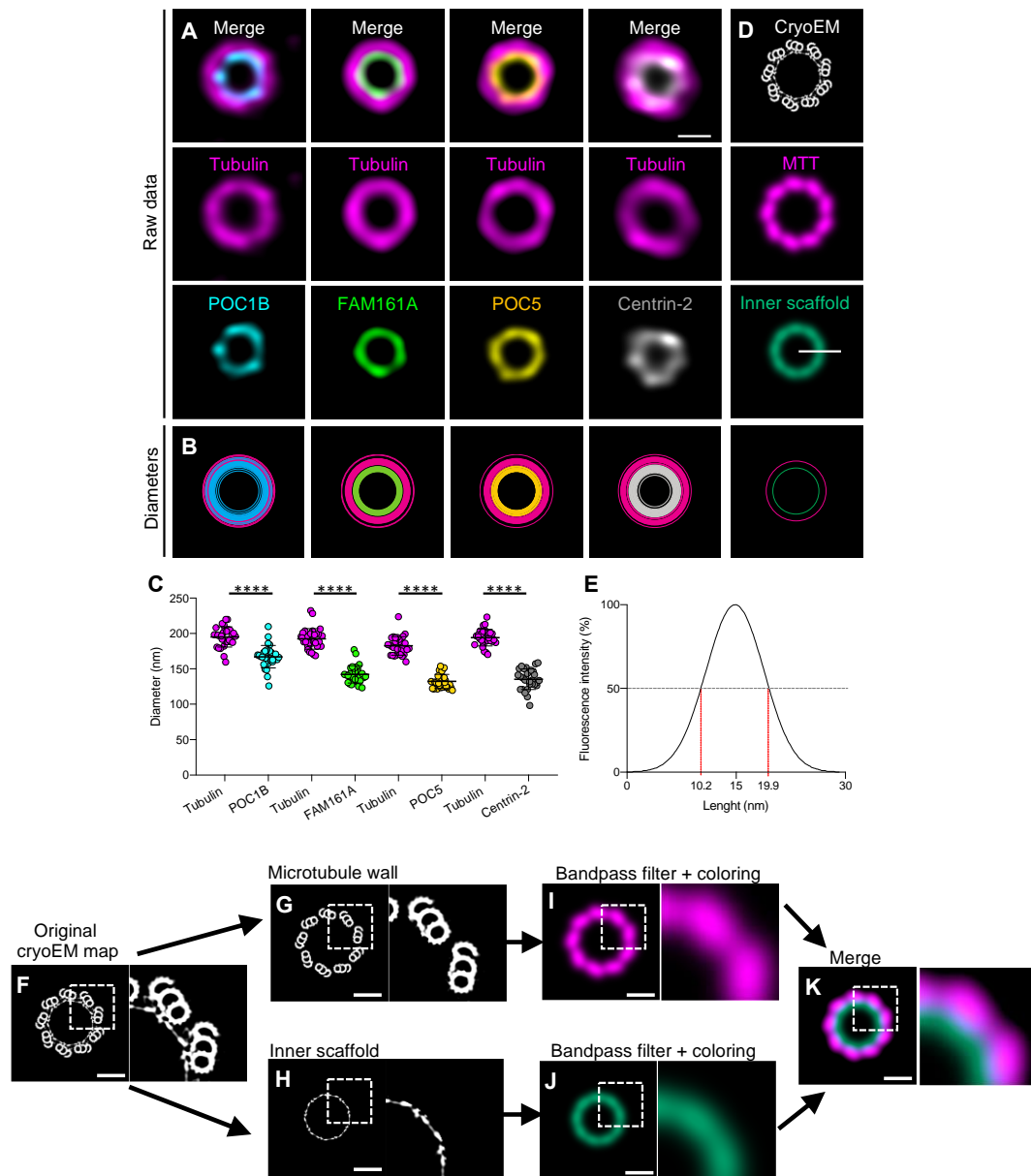


Fig. S9. POC1B, FAM161A, POC5, and Centrin-2 colocalize with the inner scaffold structure as simulated U-ExM fluorescence. (A) Representative Lightning confocal image of expanded human centrioles (top views). Cyan: POC1B; green: FAM161A; yellow: POC5; grey: Centrin-2, magenta: tubulin. Scale bar: 100 nm. (B) Plotted individual diameters of tubulin and inner scaffold proteins showing variability, color code as above. (C) Quantification of tubulin (magenta) and inner scaffold protein (color code as above) diameter in nm. Average (+/- standard error of the mean) are as follows: 195 (+/-2.6) and 167 (+/-3.0) for tubulin and POC1B, 192

(+/-2.7) and 142 (+/-2.2) for tubulin and FAM161A, 183 (+/-2.4) and 132 (+/-1.8) for tubulin and POC5, 194 (+/-2.2) and 135 (+/-2.7) for tubulin and Centrin-2. N=29, 30, 30, 29 centrioles for POC1B, FAM161A, POC5 and Centrin-2, respectively from 3 independent experiments. Statistical significance was assessed by one-way ANOVA followed by Tukey's posthoc test, ****= $p < 0.0001$ for each condition. **(D)** Cryo-EM map of a *Paramecium* centriole showing the MTTs and inner scaffold, with its corresponding U-ExM fluorescent model below (see panels F-K for the generation of this model). Magenta: MTT; cyan: inner scaffold. White line corresponds to the plot profile shown in **E**. **(E)** Plot profile used to measure the width of the modeled inner scaffold fluorescent signal (related to Figure 4K). **(F)** 2D projection from the reconstructed cryo-EM map, showing the centriolar central core, containing MTTs and the inner scaffold. **(G)** 2D projection of MTTs segmented from the original cryo-EM map. **(H)** 2D projection of the inner scaffold segmented from the original cryo-EM map. **(I, J)** After rescaling to U-ExM dimensions, a bandpass filter was applied to the maps at 140nm resolution to simulate the confocal imaging after U-ExM treatment. Note that the colors are added to mimic the fluorescent signal. **(K)** Merge of the filtered MTT (panel **I**, magenta) with the filtered inner scaffold (panel **J**, cyan). Scale bars: 400 nm.

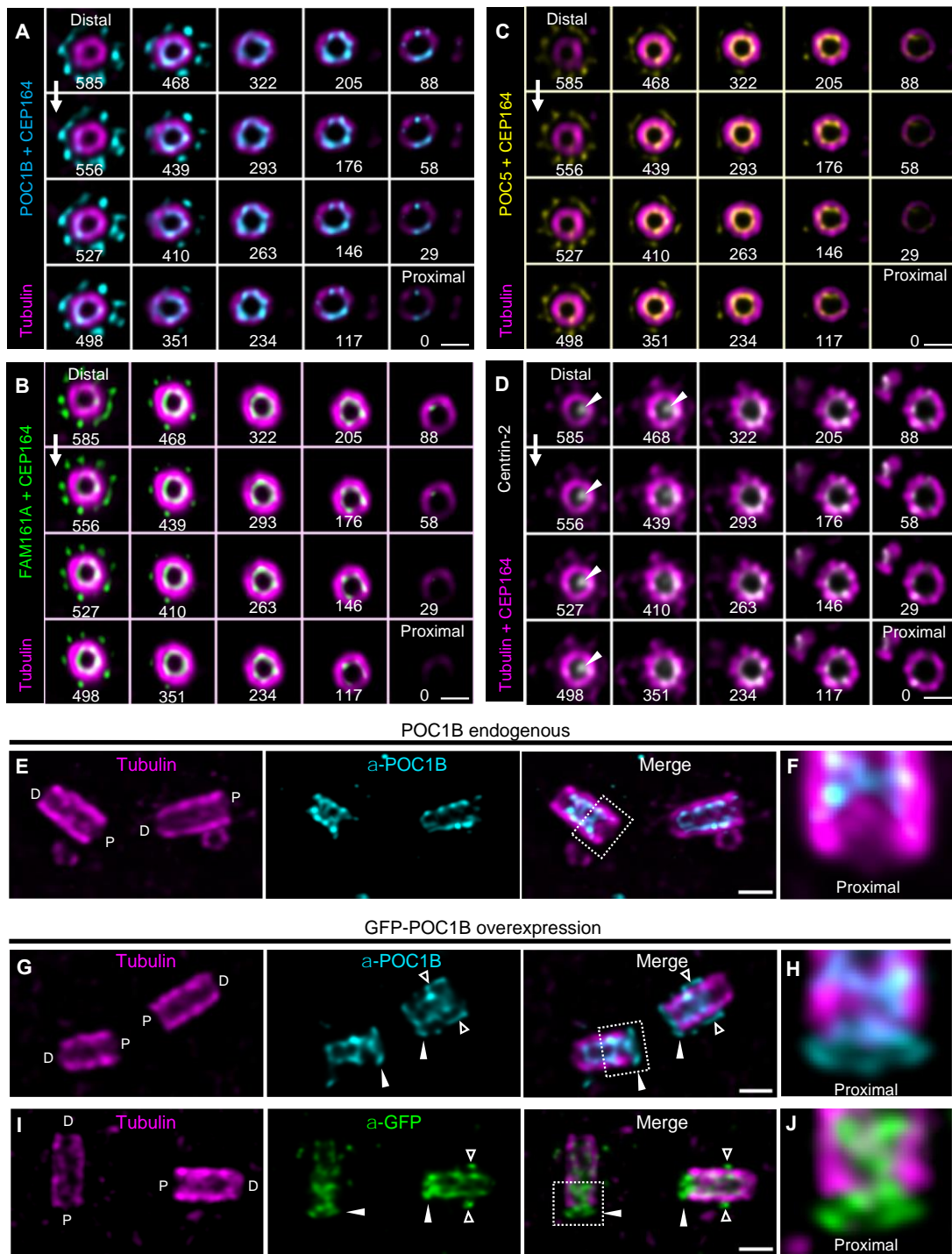


Fig. S10. 3D localization of the inner core proteins and extended localization of GFP-POC1B at the proximal region of the centriole upon overexpression. (A, B, C, D) Top view 3D images of expanded mature human centrioles stained with tubulin (magenta), POC1B (cyan) or FAM161A (green), POC5 (yellow) or Centrin-2 (gray) and Cep164 (centriolar distal appendage marker). 3D volumes are shown as serial

cross-sections through the centrioles, with z-height indicated in each image. White arrowheads indicates an additional dot-like localization of Centrin-2 at the distal tip. Z-steps every 120 nm. Scale bar: 250 nm. Representative images from 3 independent experiments. **(E)** Human centrosome imaged by U-ExM, stained with tubulin (magenta) and POC1B (cyan). D: distal end, P: proximal end. Scale bar: 230 nm. **(F)** Enlarged view of dashed region in panel **E**. Note that POC1B is absent from the proximal region. **(G and I)** U-ExM of a human centrosome after 24 hours of GFP-POC1B overexpression. Scale bar: 245 nm. The antibody against POC1B (cyan) recognized the endogenous POC1B as well as GFP-POC1B (**G**), whereas the antibody against GFP recognized only GFP-POC1B (**I**). In both cases, GFP-POC1B accumulated at the proximal side of the centriole (white arrowhead), as highlighted by the enlarged region in panels **H** and **J**. This result explains the proximal localization of GFP-POC1B reported in (40) upon overexpression. We also noticed localization near the level of the sub-distal appendages upon over-expression (open arrowhead).

Movie S1. Cryo-tomogram of a *P. tetraurelia* centriole ex vivo. Slices through a tomogram showing a *P. tetraurelia* centriole from longitudinal side view (top panel) and cross-section top view (bottom panel). The yellow line in the top panel indicates the position of the cross-section seen in bottom panel. Orange arrows: inner scaffold. Scale bar: 100 nm.

Movie S2. Cryo-tomogram of a *C. reinhardtii* centriole in situ. Slices through a tomogram showing a *C. reinhardtii* centriole from longitudinal side view (top panel) and cross-section top view (bottom panel). The yellow line in the top panel indicates the position of the cross-section seen in bottom panel. Orange arrows: inner scaffold. Scale bar: 100 nm.

Movie S3. 3D representation of the *P. tetraurelia* central core highlighting the helical pattern of the inner scaffold. One helix turn of the inner scaffold is highlighted in light pink, and the next helix turns are dark pink. MTTs are in purple, and the inner scaffold is in orange.

Movie S4. 3D representation of the *C. reinhardtii* central core highlighting the helical pattern of the inner scaffold. One helix turn of the inner scaffold is highlighted in light pink, and the second turn is dark pink. MTTs are in purple, and the inner scaffold is in orange.

Movie S5. 3D rendering of the full central core architecture from *P. tetraurelia*.

Top view (left) and side view (right) of the reconstructed central core of *P. tetraurelia*. The side view shows slices through from the external surface to the internal core of the centriole. MTTs are in purple, and the inner scaffold is in orange.

Movie S6. 3D rendering of the full central core architecture from *C. reinhardtii*.

Top view (left) and side view (right) of the reconstructed central core of *C. reinhardtii*. The side view shows slices through from the external surface to the internal core of the centriole. MTTs are in purple, and the inner scaffold is in orange.

Data file S1. The complete central core reconstruction from *P. tetraurelia*. The contrast is inverted, with the protein densities in white.

Data file S2. The complete central core reconstruction from *C. reinhardtii*. The contrast is inverted, with the protein densities in white.